EXPERIMENT AND SIMULATION STUDIES ON THERMAL PERFORMANCE OF A NOVEL WATER-COOLING PREMIXED WALL-HUNG GAS BOILER

by

Ning WANG, Shifeng DENG, Zongyi WANG, Yong GUI, Ming LE, Qinxin ZHAO, and Huaishuang SHAO*

Key Laboratory of Thermo-Fluid Science and Engineering,
Xi'an Jiaotong University, Xi'an, China

Original scientific paper
https://doi.org/10.2298/TSCI221017067W

A wall-hung gas boiler was innovatively proposed and designed in this paper. Water-cooling premixed combustion and enhanced condensation heat exchange technology were adopted in the boiler. The extruded aluminum plate-fin structure was adopted in the burner and condensing heat exchanger. Experiment and numerical simulation studies were conducted on the flow, combustion, and heat exchange characteristics of the boiler. The effect of the fin structure, excess air coefficient, heat load, and water-cooling temperature on the thermal performance of the boiler was analyzed. The results showed that reliable ignition, stable combustion, uniform flame distribution, and low pollutant emissions can be achieved in the wall-hung gas boiler. Affected by burning intensity and internal flue gas re-circulation, when the burner plate-fin gap was 1.63 mm, the flame was the shortest and the NO_x emissions were the lowest. Under this fin condition, ultra-high efficiency and ultra-low emissions can be achieved in the boiler with a low excess air coefficient. When the excess air coefficient was 1.3, the NO_x emissions were less than 30 mg/m^3 at the heat load of 4-14 kW, and the thermal efficiency can reach up to 102.8% at the rated load of 14 kW. Within the scope of the experiment, the NO_x emissions changed little with the water-cooling temperature. At the temperature of 333 K, there was still a great NO_x emission reduction effect.

Key words*: wall-hung boiler, water-cooling premixed combustion, condensing heat exchange, extruded aluminum*

Introduction

Water-cooling premixed combustion is a new gas combustion technology with broad development prospects. This technology has the advantages of uniform combustion and low pollutant emissions. Because the low NO_x emissions are achieved by cooling the flame root, the excess air coefficient during combustion is low. The thermal efficiency is thus higher than that of the usual premixed boiler. Some scholars [1, 2] transformed conventional boilers into water-cooling premixed boilers. They found that the NO_x emissions of the transformed boiler decreased significantly to about 20 mg/m^3, and the excess air coefficient was low. At present, water-cooling premixed combustion technology is mostly used in industrial boilers but rarely used in wall-hung boilers.

* Corresponding author, e-mail: shaohs@xjtu.edu.cn

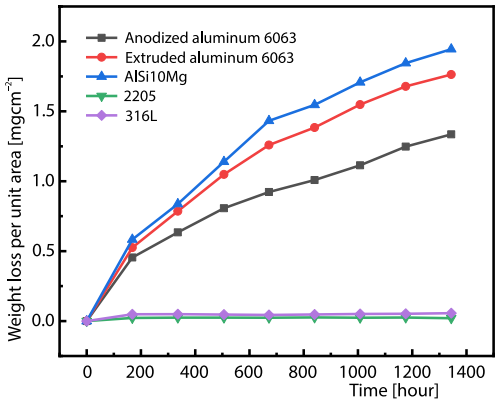

Figure 1. Corrosion kinetics curves of five materials under 60 °C natural gas condensate environment

In addition, the advanced condensing heat exchanger for wall-hung boilers is mainly made of cast aluminum-silicon alloy or stainless steel. For the cast aluminum-silicon, in the casting process, the environmental protection requirements are strict, and the molds are expensive. For the stainless steel, the heat exchange efficiency is low. Extruded aluminum is a mature technology in China, it has the advantages of simple production process and low investment cost. Besides, extruded aluminum has high heat exchange coefficient and fairly strong corrosion resistance, as shown in fig. 1.

In this paper, we proposed and designed a novel wall-hung boiler, in which the burner and heat exchanger adopted extruded aluminum plate-fin structure. The boiler can achieve ultra-low emissions at low excess air coefficient. And the heat exchange is enhanced, so ultra-high efficiency can be achieved. The structure of the boiler has important practical significance in the application of wall-hung boilers.

Many scholars carried out studies on combustion and heat exchange, which have a significant guiding role in the design of the gas boiler. Moghaddam *et al*. [3] designed a premixed porous plate burner and found that the addition of the flow distribution plate reduced the NO_x emissions. Yu *et al.* [4] found that the larger the burner porosity, the higher the thermal efficiency and the NO_x emissions, and the lower the CO emissions. Hassan *et al*. [5] found that the lower the temperature of the inlet mixture, the lower the CO and NO emissions of the boiler. Lin *et al*. [6] found that for water-cooling combustion, with the Reynolds number of the cooling water increased, the NO_x emissions decreased, the CO emissions increased, and the overall efficiency decreased. Wang *et al*. [7] conducted numerical optimization of a side-wall burner, and studied the effect of the burner structure on CO and NO_x emissions. Aleksandar *et al*. [8] established a performance prediction and optimization model on burner geometry and operating parameter. Many scholars studied the thermal-hydraulic characteristics of the heat exchanger with different fin structures and got a good heat exchange effect [9-13]. Cai *et al*. [14] found that when the exhaust gas temperature of the boiler is 160 °C, the thermal efficiency decreased by about 0.95% when the excess air coefficient increased by 0.2. Wang *et al*. [15] found that when the boiler operated from 30% load to 75% load, the flue gas re-circulation rate was reduced by 4.9%. When the load continued to increase, the re-circulation rate remain unchanged. Chen *et al*. [16] found that the NO_x emissions increased with the increase of the boiler load. With the increase of excess air coefficient, the NO_x emissions first increased and then decreased. The NO_x emissions decreased with the increase of flue gas re-circulation rate. Zhu *et al*. [17] found that the temperature and NO_x emissions do not change monotonically with excess air coefficient, but decrease monotonically with flue gas re-circulation rate.

Firstly, a novel condensing wall-hung gas boiler structure was introduced. The water-cooling premixed combustion was adopted in the boiler. The burner and condensing heat exchanger were made of extruded aluminum plate fins. Secondly, the experiment on combustion and heat exchange characteristics was carried out. The results showed that the wall-hung boiler had significant energy-saving and emission-reduction advantages compared with the existing wall-hung boilers on the market. Finally, the numerical simulation was conducted on

the flow and combustion characteristics of the water-cooling burner and the furnace. The effect of the structure and operating parameters on the flame length, internal flue gas re-circulation rate, and flue gas temperature at the furnace outlet was obtained.

Structure of the wall-hung boiler

This section introduces the structure of the condensing wall-hung gas boiler. The design conditions are the heat load is 14 kW, the excess air coefficient is 1.3, the inlet and outlet water temperatures in the boiler are 303/323 K, respectively, and the thermal efficiency is 103%.

Overall structure

As shown in fig. 2, the boiler includes a gas distribution structure, plate-fin water-cooling burner, water-jacketed furnace, plate-fin condensing heat exchanger, flue gas duct, *etc.* The natural gas and air enter the gas distribution structure after being mixed by a fan. After the mixed gas is evenly distributed, it is ejected from the gap of the burner fins. Then the mixture is ignited and burned in the furnace. After the heat is released in the furnace and condensing heat exchanger, the flue gas is discharged from the flue gas duct. The cold water first enters the condensing heat exchanger. After absorbing the vaporization latent heat and a large amount of sensible heat, it enters the water-cooling burner to cool the flame root. Finally, it enters the furnace to further absorb the heat. Then it is discharged from the outlet of the furnace water channel, producing hot water.

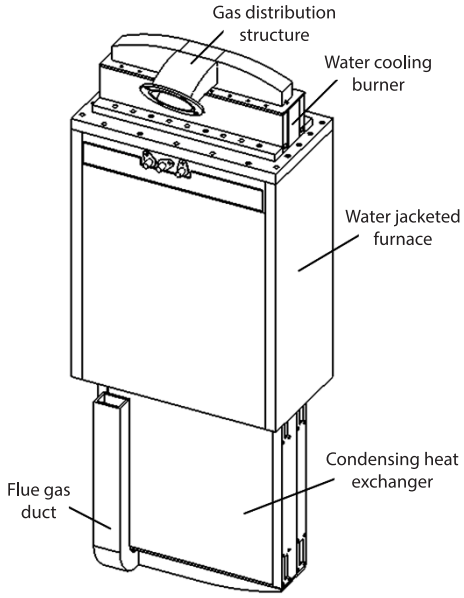

Figure 2. The overall structure of the wall-hung boiler

Gas distribution structure

The gas distribution structure is shown in fig. 3. The mixed gas enters from the middle and is distributed to both sides. The distribution of the mixed gas is mainly realized through the deflector and the orifice plate. The 64 rows and 7 columns of circular nozzle holes are evenly arranged on the orifice plate. The deflectors are symmetrical on the left and right and avoid the position of the orifice.

The sizes of the orifice plate are shown in tab. 1. The gas distribution structure has a great velocity distribution effect and load adaptability. Its resistance is low.

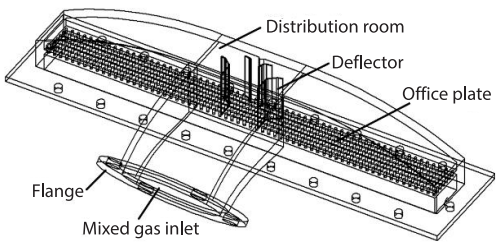

Figure 3. Gas distribution

Table 1. Orifice plate sizes

Parameter	Symbol	Value	Unit
Orifice diameter	d	1.2	[mm]
Orifice plate length	a	229.5	[mm]
Orifice plate width	b	22	[mm]
Hole row number	Z_1	7	1
Hole column number	Z_2	64	1
Orifice plate thickness	e	3	[mm]

Burner

As shown in fig. 4, the burner is composed of a pair of small water-cooling plates and plate fins.

The small water-cooling plate clamps the pair of plate fins by bolting. Their contact surfaces are evenly filled with thermal grease. The water inside the small water-cooling plate flows up and down along the *S*-shaped channel. The sizes of three pairs of fins are shown in fig. 5. Their height and slot area are the same. The three plate-fin gaps are 0.53 mm, 1.63 mm, and 2.65 mm, respectively. The plate-fin depth is 55 mm. At the rated load of 14 kW, the mixed gas velocity at the outlet of the gap is about 2.65 m/s.

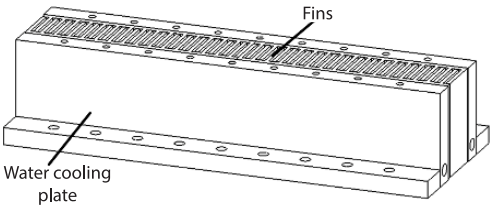

Figure 4. Burner structure

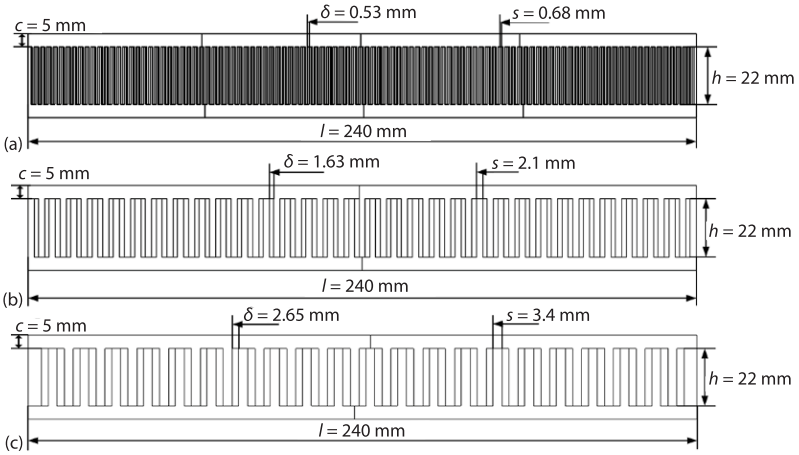

Figure 5. Burner plate fin structure and sizes; (a) Fin 1, (b) Fin 2, and (c) Fin 3

Furnace and heat exchanger

The furnace structure and its basic sizes are shown in fig. 6. The furnace is composed of four aluminum water cooling plates, upper and lower cover, a fire window, ignition needles, and other components. The water flows from bottom to top along the *S*-shaped channel. The width of the inlet and outlet of the furnace is smaller than that of the section of the furnace.

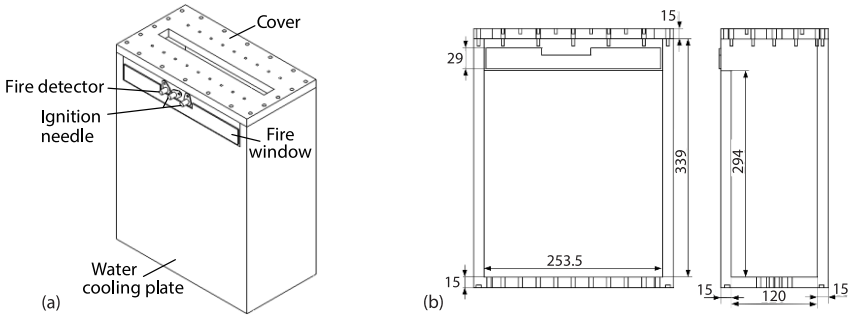

Figure 6. Furnace structure (a) and sizes (b)

As shown in fig. 7, the heat exchanger is centrosymmetric and consists of two oppositely inserted flue plates and waterside cover plates. There are 32 thin vertical plate fins on the flue board, which form a vertical gas-flow channel after being inserted into each other. The flue gas-flows from top to bottom. After the waterside cover plate and the flue plate are assembled, the *S*-shaped channel is formed. The water flows from bottom to top. The burner fins and condensing heat exchanger are extruded from EN AW-6063 aluminum profiles.

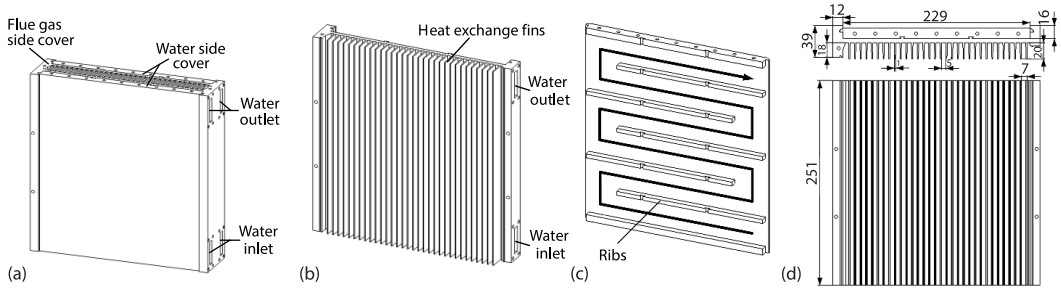

Figure 7. Condensing heat exchanger structure and sizes; (a) overall structure, (b) flue board structure, (c) water side cover structure, and (d) flue board sizes

Experiment studies on combustion and heat exchange of the wall-hung boiler

Experiment system and instrument

To explore the performance of the wall-hung boiler, we conducted an experiment on combustion and heat exchange. The experiment system and test bench are shown in fig. 8. After the natural gas and air are mixed and distributed evenly, the mixed gas enters the furnace for combustion and heat exchange. After further heat exchange in the condensing heat exchanger, the flue gas is discharged. The cold water enters the condensing heat exchanger, the burner, and the furnace in turn. The water discharged from the furnace enters the plate heat exchanger and releases heat to the cooling water, and then returns to the condensing heat exchanger to form an internal water circulation.

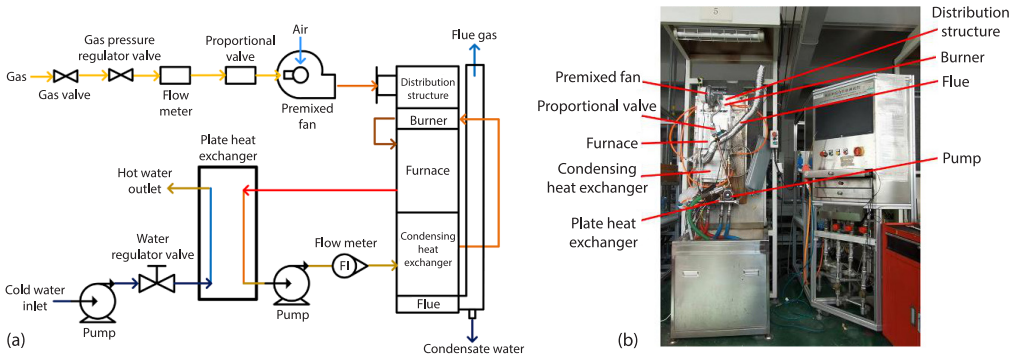

Figure 8. Experimental system (a) and test bench (b)

Experimental method and process

Experimental method

During the experiment, we ensured that the natural gas pressure was 2000 ±20 Pa, the laboratory temperature was 293 ±5 K, and the water pressure was 100 ±50 kPa. The water cooling temperature refers to the average temperature at the inlet and outlet of the small water cooling plate. After stable combustion for 10 minutes and the measuring value is stable, we recorded the results. Three tests were conducted for each working condition and the average value was taken as the final result. The 12T pipe-line natural gas in China was chosen as the fuel. The composition and properties of the experimental natural gas are shown in tab. 2.

Table 2. Natural gas composition and properties (288 K, 101.3 kPa)

Composition	Methane (CH_4)	Ethane (C_2H_6)	Propane (C_3H_8)	Isobutane (i-C_4H_{10})	n-butane (n-C4H10)
Content [%]	97.033	2.065	0.453	0.447	0.64
High calorific value [MJm^{-3}]	39.8381	Low calorific value [MJm^{-3}]	35.9260	Relative density	0.5895

Table 3. The type and accuracy of the measuring instruments

Instrument	Model	Accuracy
Flue gas analyzer	Testo330-1	0.1 ppm
Thermocouple	K	0.1 K
Digital thermometer	DT-1310	0.1 K
Gas turbine flow meter	LWQ-25	±1.5% R
Electromagnetic water flow meter	GK-LDE	±0.5% R
Temperature and humidity sensor	HIOKI 3641	±0.5 K, ±5% RH
Electronic scale	Bai Jie SF-400	0.1 g
Stopwatch	PC894	0.01 seconds

The type and accuracy of the measuring instruments used in the experiment are shown in tab. 3. The excess air coefficient of 1.3, the heat load of 10 kW, and the water-cooling temperature of 318 K were selected as the basic working condition. Single-factor and orthogonal experiments were carried out to explore the combustion and heat exchange characteristics of the boiler.

Data processing

According to GB 25034-2020 (gas-fired heating and hot water combi-boiler), the data processing process is as follows.

The heat load calculation during the experiment:

$$Q = \frac{1}{3.6} q_{vg} H_l \frac{101.3 + p_m}{101.3} \sqrt{\frac{T_{air}}{293.15} \frac{288.15}{T_g} \frac{d_t}{d_r}} \tag{1}$$

where Q [kW] is the heat load, q_{vg} [m^3 per hour] – the natural gas-flow, H_l [MJm^{-3}] – the low calorific value of the fuel, p_m [kPa] – the natural gas pressure, T_{air} and T_g [K] are the temperature of the air and the natural gas, respectively, d_t – the relative density of the dry test gas, and d_r – the relative density of the dry reference gas.

The excess air coefficient was calculated by the oxygen content of the exhaust. The conversion method of oxygen content and excess air coefficient:

$$\alpha = \frac{1}{1-\frac{\omega}{21}} \tag{2}$$

where α is the excess air coefficient and ω [%] is the volume fraction of oxygen in the exhaust.

The thermal efficiency calculation:

$$\eta = \frac{4.186 \times q_{\mathrm{vm}} \times \rho_{\mathrm{s}} \times (T_2 - T_1) \times T_{\mathrm{g}} \times 101.325}{103 \times q_{\mathrm{vg}} \times H_1 \times (p_0 + p_{\mathrm{m}} - p_{\mathrm{s}}) \times 288.15} \tag{3}$$

where η [%] is the thermal efficiency of the boiler, q_{vw} [m^3 per hour] – the circulating water flow, ρ_{s} [kgm^{-3}] – the circulating water density, T_2 [K] – the water temperature at the furnace outlet, T_1 [K] – the water temperature at the inlet of the heat exchanger, p_0 [Pa] – the atmospheric pressure, p_{m} [Pa] – the natural gas pressure, and p_{s} [Pa] – the saturated water vapor pressure at T_{g}.

The relative errors of the main parameters in the experiment are shown in tab. 4.

Table 4. Experimental error analysis

Physical parameters	Relative error [%]	Physical quantity	Relative error [%]
Water flow [m^3 per hour]	0.5	Water pressure [MPa]	1
Gas-flow [m^3 per hour]	1.5	Gas pressure [MPa]	1
Water temperature [K]	0.1	Oxygen content [%]	0.2
Gas temperature [K]	0.1	Load [kW]	1.8
Exhaust temperature [K]	0.1	Thermal efficiency [%]	1.9

Experimental results and analysis

The experimental prototype ignites reliably and burns stably at 4-14 kW under the three plate-fin conditions. The flame distribution is uniform and the CO emissions are maintained within 0-11.65 mg/m^3. Other characteristics are described as follows.

Effect of excess air coefficient on the combustion and heat exchange characteristics

As shown in fig. 9, the exhaust temperature, thermal efficiency, and NO_x emissions decrease with the increase of excess air coefficient. This is because as the excess air coefficient increases, the furnace temperature and the heat exchange temperature difference decrease. When the excess air coefficient is lower than 1.3, the exhaust temperature and the NO_x emissions are the lowest, and the thermal efficiency is the highest at Fin 2. This is attributed to the moderate flue gas re-circulation rate and burning intensity at Fin 2. When the excess air coefficient is 1.5, the NO_x emissions of plate Fin 2 are only 10 mg/m^3.

Effect of heat load on the combustion and heat exchange characteristics

As shown in fig. 10, with the heat load increases, the exhaust temperature first decreases and then increases, and the thermal efficiency first increases and then decreases. This is because as the heat load increases, the flue gas temperature at the furnace outlet increases, and the heat exchange temperature difference in the condensing heat exchanger increases. To

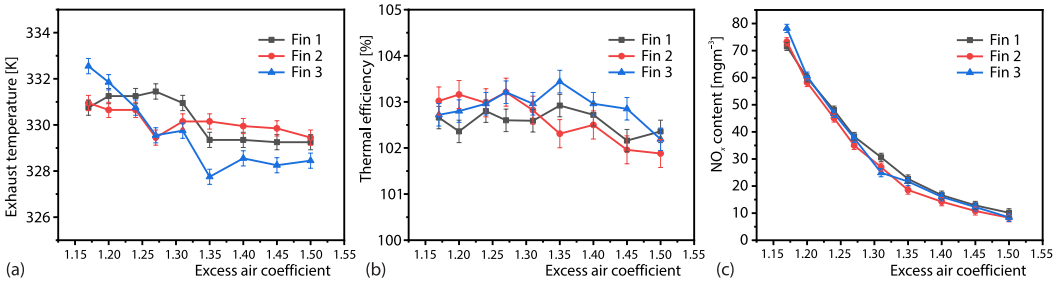

Figure 9. Effect of excess air coefficient on the combustion and heat exchange characteristics; (a) exhaust temperature, (b) thermal efficiency, and (c) NO_x emissions

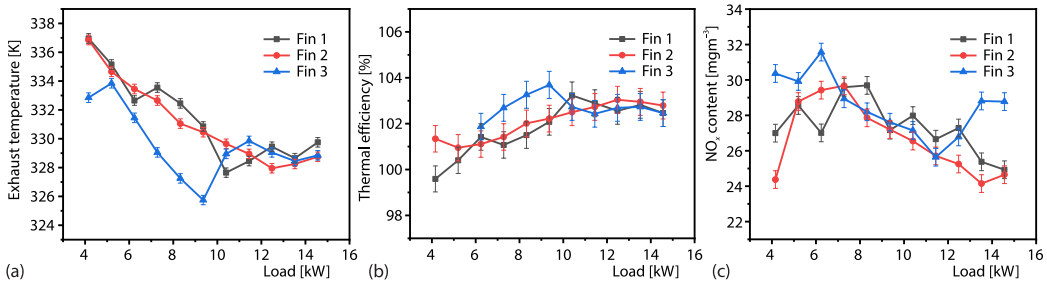

Figure 10. Effect of heat load on the combustion and heat exchange characteristics; (a) exhaust temperature, (b) thermal efficiency, and (c) NO_x emissions

maintain the water-cooling temperature at 318 K, the circulating water flow rate needs to be increased, and the heat exchange in the heat exchanger increases. Affected by the flue gas temperature and heat exchange, the exhaust temperature and thermal efficiency show a trend of segmental change. And affected by the flame length, flue gas re-circulation, and burning intensity, the NO_x emissions vary with the heat load in three-stages. The NO_x emissions are the lowest at Fin 2. Under the basic working condition of Fin 2, the exhaust temperature is 328.8 K, the thermal efficiency is 102.8%, and the NO_x emissions are 24.6 mg/m^3. When the heat load ranges from 4-14 kW, the NO_x emissions at Fin 2 are always less than 30 mg/m^3.

Effect of water-cooling temperature on the combustion and heat exchange characteristics

As shown in fig. 11, within the scope of the experiment, as the water-cooling temperature increases, the exhaust temperature increases significantly, the thermal efficiency decreases significantly, and the NO_x emissions increase slowly. This is because the water cooling

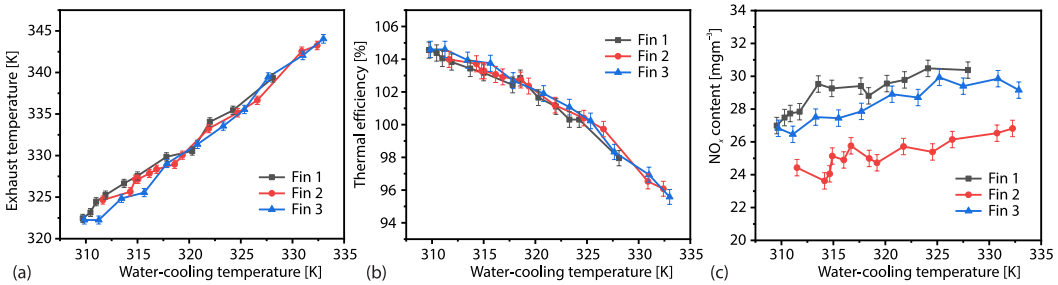

Figure 11. Effect of water-cooling temperature on the combustion and heat exchange characteristics; (a) exhaust temperature (b) thermal efficiency, and (c) NO_x emissions

temperature affects the furnace temperature and heat exchange temperature difference. In the process of the water-cooling temperature changes, the difference between the three fins is small in exhaust temperature and thermal efficiency. The NO_x emissions are the lowest under the Fin 2 condition.

Simulation studies on flow and combustion characteristics of the wall-hung boiler

Mesh and boundary conditions

We conducted the numerical simulation better explain the experiment conclusion. The numerical calculation was carried out in FLUENT and the mesh was built in FLUENT meshing. The unstructured hexahedral mesh of the 1/4 model on the burner and furnace was performed. The physical model and mesh-independent results are shown in fig. 12. The temperature distribution on the axis of the model was used to evaluate the mesh independence. It can be seen from fig. 12(b) that the mesh independence is great when the grid number is 2.42 million. We select the 2.42 million grids to conduct the simulation of the flow and combustion characteristics. The minimum size of the grid is 0.005 mm, the maximum size is 2 mm, and the number of the boundary-layer is 20. The parts with large curvature and small size are encrypted. The mesh quality is great and the y^+ is between 30-100. The local mesh is shown in fig. 13(a).

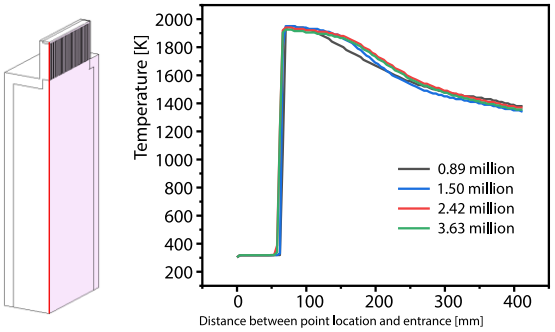

Figure 12. Model and mesh independence; (a) physics model and (b) mesh independence

The model boundary conditions are set as follows. The standard k-ε model, standard wall functions, energy equation, DO radiation model, and species transport model were selected. The methane-air two-step reaction was selected to obtain the temperature field. The *Thermal* NO_x and *Prompt* NO_x were turned on obtain the NO_x emissions. The solid material is EN AW-6063-T6 specified in European standard EN12020-1-2021. The density is 2700 kg/m^3. The specific heat capacity is 900 J/kgK. The thermal conductivity is 201 W/mK. The solid absorptivity and emissivity were set to 0.8. The flue gas absorption and emissivity were set to 0.3. The inlet of the mixed gas was set as the velocity inlet of 1.13 m/s at the rated load. The temperature of the inlet mixed gas was set to 303 K. The inlet hydraulic diameter was

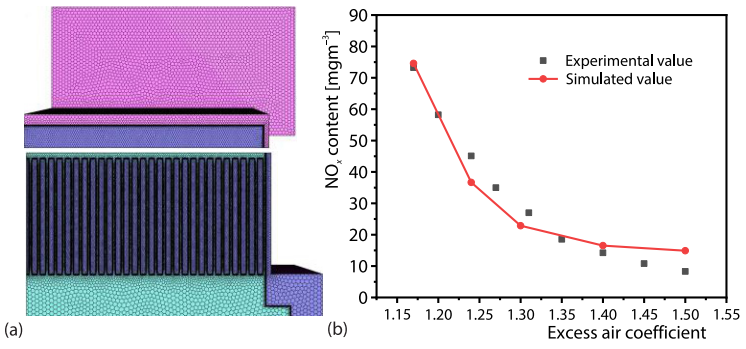

Figure 13. Local mesh and numerical model verification; (a) local mesh and (b) numerical model verification

40.15 mm. The inlet mixture composition was set according to the excess air coefficient. The outlet of the mixed gas was set as the pressure outlet of 0 Pa. The outlet hydraulic diameter was 163 mm. The waterside wall temperatures of the small water-cooling plate and the furnace were set. The temperature of the furnace wall was obtained by thermal calculation from the temperature of the small water-cooling plate. The SIMPLE algorithm and the second-order upwind style were used. The calculation was considered to have converged when the residual was less than $1 \cdot 10^{-6}$ and the average temperature as well as the mass fraction of NO in the exit section were stable.

The simulation results of the NO_x content variation at the furnace outlet with the excess air coefficient at plate Fin 2 were compared with the experimental data. The results of the comparison are shown in fig. 13(b). It can be seen that within the simulation range, the difference between the simulated values of the NO_x emissions and the experimental values is small. The simulation method can be considered accurate for the simulation work.

Data processing

In the simulation, the flame length, internal flue gas re-circulation rate, and flue gas temperature at the furnace outlet were selected to evaluate the flow and combustion characteristics.

The flame length is determined from the temperature contour on the symmetrical plane of the furnace's narrow side. The average value of the maximum contour temperature under different working conditions was selected as the flame front temperature and the temperature is 1758 K. We took the length of the region where the temperature was higher than 1758 K as the relative length of the flame [18].

The internal flue gas re-circulation rate on a certain section is calculated:

$$Kv = \frac{-\int \rho v_z \mathrm{d}A_-}{\left(\int \rho v_z \mathrm{d}A_+ + \int \rho v_z \mathrm{d}A_-\right)} \times 100\% \tag{4}$$

where K_v [%] is the flue gas re-circulation rate in a certain section, ρ [kg/m^3] – the density of flue gas, v_z [ms^{-1}] – the velocity of the flue gas in the vertical section direction, A_+ and A_- [m^2] are the area of the mainstream zone and the backflow zone of the flue gas, respectively.

The section with the largest gas backflow velocity was selected to calculate the re-circulation rate. The furnace outlet temperature refers to the mass-flow average temperature.

Results and discussion

Clear flame profiles can be captured in the simulation results. The furnace temperature is 800-1300 K. The flue gas-flow rate in the furnace is 0-6 m/s.

Effect of excess air coefficient on flow and combustion characteristics

As shown in fig.14, the profile of the flame can be clearly seen in the figure, and the length of the flame gradually becomes thicker and shorter. As shown in fig. 15, the flame length, internal flue gas re-circulation rate, and flue gas temperature at the furnace outlet decrease with the increase of excess air coefficient. This is because as the excess air coefficient increases, the flow rate of the mixed gas increases, and the stiffness of the flue gas increases. So the internal flue gas re-circulation rate increases, the burning intensity decreases, and the flue

gas temperature decreases. The gap of the Fin 1 is the smallest, the burning intensity is the largest, and the flue gas temperature is the highest. The gap of the Fin 3 is the largest, the gas-flow stiffness is the smallest, and the re-circulation rate is the highest. When the re-circulation rate is too low, the preheating effect on the unburned gas is poor and the flame is longer. When the re-circulation rate is too high, the recirculated flue gas elongates the flame. Because the internal flue gas re-circulation rate of the Fin 2 is moderate, the flame at Fin 2 is the shortest.

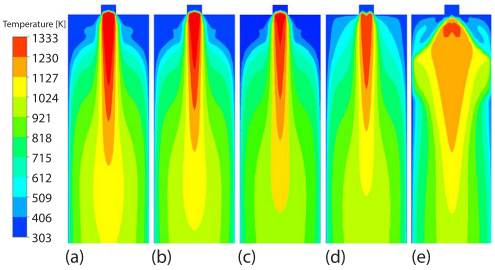

Figure 14. Variation of temperature distribution with excess air coefficient on symmetrical plane of combustion model at Fin 1

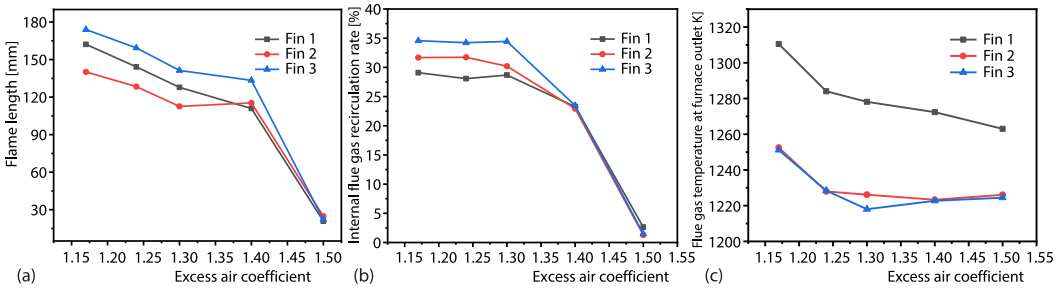

Figure 15. Effect of excess air coefficient on flow and combustion characteristics; (a) flame length, (b) internal flue gas re-circulation rate, and (c) flue gas temperature at the furnace outlet

Effect of heat load on flow and combustion characteristics

As shown in fig. 16, the flame length and flue gas temperature at the furnace outlet increase rapidly with the increase of the heat load. The internal flue gas re-circulation rate decreases with the increase of the heat load. This is because as the load increases, the heat release of the chemical reaction increases, resulting in an increase in flame length and the flue gas temperature. With the increase of the heat load, the amount of the flue gas increases, the stiffness of mainstream flue gas increases, and the effect of internal flue gas re-circulation decreases accordingly. In the process of changing with the load, the magnitude relationship of each parameter under the three fin conditions is the same as that with the change of excess air coefficient. The flame length at the rated load of plate Fin 2 is 172 mm.

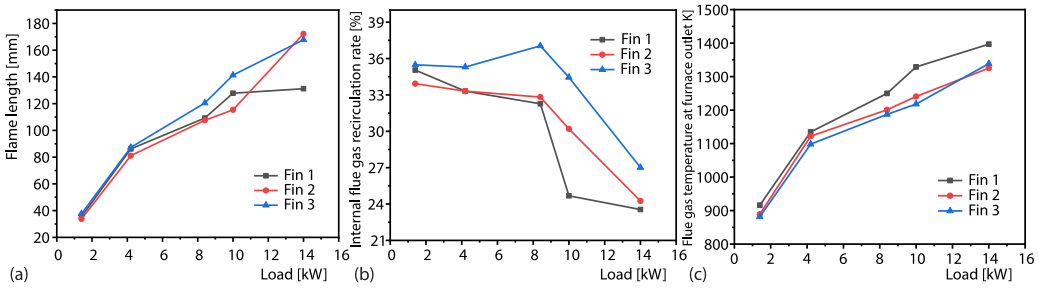

Figure 16. Effect of heat load on flow and combustion characteristics; (a) flame length, (b) internal flue gas re-circulation rate, and (c) flue gas temperature at the furnace outlet

Effect of water-cooling temperature on flow and combustion characteristics

As shown in fig. 17, within the scope of the simulation, the flame length, the internal flue gas re-circulation rate, and the flue gas temperature at the furnace outlet increase slowly with the increase of the water-cooling temperature. This is because as the water-cooling temperature increases, the preheated effect on the mixed gas becomes stronger, the density of the mixed gas decreases, and the flow rate increases. The flame length, the internal re-circulation effect, and the temperature of the flue gas increase accordingly. In the process of changing with water-cooling temperature, the magnitude relationship of each parameter under the three fin conditions is the same as that with the change of excess air coefficient.

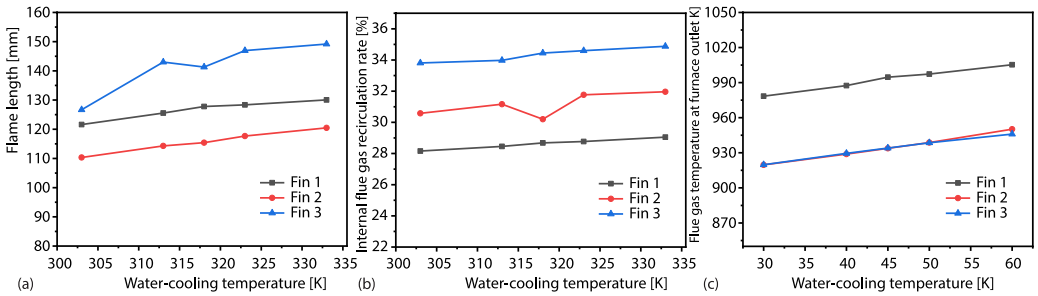

Figure 17. Effect of water-cooling temperature on flow and combustion characteristics; (a) flame length, (b) internal flue gas re-circulation rate, and (c) flue gas temperature at the furnace outlet

Conclusions

- Reliable ignition, stable combustion, and uniform flame distribution can be achieved in the designed extruded aluminum water-cooling premixed condensing wall-hung gas boiler. The CO emissions during the combustion process are always less than 11.65 mg/m^3.
- The flame length and NO_x emissions of water-cooling premixed combustion are affected by the plate fin. When the plate-fin gap is 1.63 mm, the flame is the shortest and the NO_x emissions are the lowest. Under the basic condition of the rated load of 14 kW, excess air coefficient of 1.3, and water-cooling temperature of 318 K, the flame length is only 172 mm, the NO_x emissions are only 24.6 mg/m^3.
- The NO_x emissions of the boiler can be significantly reduced by the water-cooling premixed combustion. At the normal excess air coefficient of 1.5, the NO_x emissions can be reduced to 10 mg/m^3.
- Ultra-high efficiency and ultra-low emissions are achieved in the wall-hung boiler with a low excess air coefficient. Based on the current 30 mg/m^3 NO_x emission standard, the excess air coefficient of the prototype can be reduced to 1.3 at 4-14 kW load through 318 K water-cooling fins. The thermal efficiency can reach up to 102.8% at the rated load of 14 kW.

Acknowledgment

This article is supported by the Key Research and Development Program of Shaanxi Province (2021GXLH-Z-005) and the National Natural Science Foundation of China (51876165). Thanks to *Guangdong Shengkai Thermal Energy Equipment Co., Ltd.* for its strong support of the experiment.

References

[1] Chen, Y., *et al*., Comparative Analysis of Application Effect on Low-Nitrogen Combustion Technology For Small Gas Boilers (in Chinese), *District Heating*, (2019), pp. 54-56+87
[2] Zhu, J., *et al*., Application of Water-Cooling Premixed Vacuum Hot Water Boiler in Low-Nitrogen Transformation of Boilers in a District in Beijing (in Chinese), *District Heating*, (2018), 04, pp. 58-60+78
[3] Moghaddam, M. H. S., *et al*., Numerical Study of Geometric Parameters Effecting Temperature and Thermal Efficiency in a Premix Multi-Hole Flat Flame Burner, *Energy*, *125* (2017), Apr., pp. 654-662
[4] Yu, B., *et al.*, Effects of Exhaust Gas Re-Circulation on the Thermal Efficiency and Combustion Characteristics for Premixed Combustion System, *Energy*, *49* (2013), Jan., pp. 375-383
[5] Hassan, G., *et al*., Reduction in Pollutants Emissions from Domestic Boilers-Computational Fluid Dynamics Study, *Journal of Thermal Science and Engineering Applications*, *1* (2009), 1, 011007
[6] Lin, Z., *et al.*, Experiment on the Effect of Wall Micro-Channel Cooling on The Performance of Swirl Combustor (in Chinese), *Journal of Aerospace Power*, *34* (2019), 02, pp. 376-386
[7] Wang, M. Y., *et al*., Numerical Simulation on the Emission of NO_x from the Combustion of Natural Gas in the Sidewall Burner, *Thermal Science*, *26* (2022), 1A, pp. 247-258
[8] Milivojevic, A. M., *et al*., Analysis of the Performance of A Low-Power Atmospheric Burner for Gas Appliances for Households and Their Impact on the Emission and Stability of the Burner, *Thermal Science*, *25* (2021), 3, pp. 1891-1903
[9] Lee, S., *et al*., Performances of a Heat Exchanger and Pilot Boiler for the Development of a Condensing Gas Boiler, *Energy*, *36* (2011), 7, pp. 3945-3951
[10] Dong, J., *et al*., Experimental Study on Thermal-Hydraulic Performance of a Wavy Fin-and-Flat Tube Aluminum Heat Exchanger, *Applied Thermal Engineering*, *51* (2013), 1-2, pp. 32-39
[11] Yasar, H., et al., Effect of Wavy Fin Usage on Thermal Performance of Heat Exchanger Used in Combi Boilers, *Thermal Scienc*e, *24* (2020), 2A, pp. 693-700
[12] Ganesan, S. K., *et al*., Analysis of Fin Characteristics for Overall Heat Transfer in Boiler Economizer, *Thermal Science*, *26* (2022), 2, pp. 849-855
[13] Wang, Y., *et al.*, Experimental and Numerical Studies on Actual Flue Gas Condensation Heat Transfer in a Left-Right Symmetric Internally Finned Tube, *International Journal of Heat and Mass Transfer*, *64* (2013), Sept., pp. 10-20
[14] Cai, Q., *et al.* The Research on the Influence of Boiler Operating Parameters on Thermal Efficiency, *Proceedings*, 6th International Conference on Energy, Environment and Materials Science (EEMS), Hulun Buir, China, 2020, 585
[15] Wang, X., *et al*., Analysis of the Influence of Boiler Parameters on the Flue Gas Re-Circulation Rate of the Second Reheat Unit, *Proceedings*, 2021 IEEE Sustainable Power and Energy Conference (iSPEC), Nanjing, China, 2021, pp. 2225-2230
[16] Chen, X., *et al*., The NOx Emission Performance and Operation Optimization of Low Nitrogen Burner, *Chemical Industry and Engineering Progress*, *40* (2021), 2, pp. 1069-1076
[17] Zhu, Y., *et al.*, Combustion Characteristic Study with a Flue Gas Internal and External Double Re-Circulation Burner, *Chemical Engineering and Processing-Process Intensification*, *162* (2021), 108345
[18] Xie, K., *et al.*, Numerical Study on Flame and Emission Characteristics of a Small Flue Gas Self-Circulation Diesel Burner With Different Spray Cone Angles, *Thermal Science*, *26* (2022), 1A, pp. 389-400

Paper submitted: October 17, 2022
Paper revised: February 8, 2023
Paper accepted: February 20, 2023